Solution-printable fullerene/TiS2 organic/inorganic hybrids for high-performance flexible n-type thermoelectrics

Journal:	*Energy & Environmental Science*
Manuscript ID	EE-ART-12-2017-003617.R1
Article Type:	Paper
Date Submitted by the Author:	24-Feb-2018

Complete List of Authors:	Wang, Liming; Texas A&M University College Station, Materials Science Zhang, Zimeng; Texas A&M University College Station, Materials Science Geng, Linxiao; University of California, Riverside, Department of Chemical and Environmental Engineering Yuan, Tianyu; Texas A&M University, Materials Science and Engineering Liu, Yuchen; Texas A&M University College Station, Materials Science Guo, Juchen; University of California at Riverside, Chemical and Environmental Engineering Fang, Lei; Texas A&M University, Chemistry; Texas A&M University, Materials Science and Engineering Qiu, Jenny; Texas Tech University, Wang, Shiren; Texas A&M University College Station, Materials Science

Solution-printable fullerene/TiS_2 organic/inorganic hybrids for high-performance flexible n-type thermoelectrics

Liming Wang[1], Zimeng Zhang[1], Linxiao Geng[2], Tianyu Yuan[3], Yuchen Liu[1], Juchen Guo[2], Lei Fang[3], Jingjing Qiu[4], Shiren Wang[1]*

[1]Department of Industrial and Systems Engineering, Texas A&M University, College Station, TX 77843, USA.

[2] Department of Chemical and Environmental Engineering, University of California, Riverside, CA 92521, USA.

[3]Department of Chemistry, Texas A&M University, College Station, TX 77843, USA.

[4]Department of Mechanical Engineering, Texas Tech University, Lubbock, TX77409, USA

*E-mail: s.wang@tamu.edu

Abtract

Solution-printable and flexible thermoelectric materials have attracted numerous attentions because of their scalable processibility and great potential for powering flexible electronics, but it is challenging to integrate mechanical flexibility, solution-printability and outstanding thermoelectric properties together. Particularly, such an n-type thermoelectric material is highly sought after. In this paper, 2D TiS_2 nanosheets were exfoliated from layered polycrystalline powders, and then assembled with C_{60} nanoparticles, resulting in a new class of flexible n-type thermoelectric materials via concurrent enhancement in power factor and reduction in thermal conductivity. The resultant C_{60}/TiS_2 hybrid films show ZT~0.3 at 400 K, far superior to the state-of-the-art solution-printable and flexible n-type thermoelectric materials. Particularly, such thermoelectric property rivals that of single-crystals TiS_2-based thermoelectric materials, which are expensive, difficult to synthesize, and incapable of solution printing. The solution of C_{60}/TiS_2 hybrid was also used as ink for printing large-area flexible and spatial thermoelectric devices. An outstanding output power of 1.68 W m^{-2} was generated at a temperature gradient of 20 K. This work paves the way for flexible, solution-printable, high-performance thermoelectric materials for flexible electronics.

Introduction

Thermoelectric effect, which involves direct conversion between thermal energy and electrical energy without moving parts or hazardous working fluids, has attracted increasing attentions in sustainability.[1-5] Particularly, thermoelectric materials can harvest the body heat for supplying power to the wearable electronics. Flexible thermoelectric materials without toxic or rare elements are extremely attractive and preferred, especially those solution-printable. The efficiency of energy conversion is determined by figure of merit (*ZT*) of materials, defined as $ZT = S^2\sigma T/\kappa$, where S is the Seebeck coefficient, σ is the electrical conductivity, κ is the thermal conductivity, and T is the absolute temperature. The rigid inorganic materials such as Bi_2Te_3 demonstrate high *ZT*, but lack of flexibility hinders their potential for wearable power sources. Alternatively, organic thermoelectric materials have received great attentions because of their flexibility and recent break-through in thermoelectric properties.[6-10] For example, solution-processed p-type poly(3,4-ethylenedioxythiophene) (PEDOT) based films demonstrated outstanding thermoelectric properties with $ZT > 0.25$.[6,7] Unfortunately, the developments of n-type organic thermoelectric materials significantly lags behind their p-type counterparts in terms of low electron transport properties and poor stability.[11-14]

Organic/inorganic hybrids emerge as a new class of flexible n-type thermoelectric materials; particularly, organic materials-intercalated transition metal dichalcogenides (TMD) have the great potential for flexible air-stable n-type thermoelectrics. TiS_2, one type of 2D transition metal dichalcogenides (TMDs), is a very promising candidate for n-type thermoelectrics due to the advantages including environmentally benign, chemical stability, mechanical flexibility and composed of earth-abundant elements of Ti and S.[15-18] Furthermore, TiS_2 single crystal was reported with a very high power factor (PF, $S^2\sigma$) of 3710 $\mu W\ m^{-1}\ K^{-2}$ even at room temperature, which rivaled the state-of-the-art Bi_2Te_3 alloys.[19] However, its *ZT* was rather low, only 0.16 at 300 K because of the relatively large thermal conductivity (6.8 $W\ m^{-1}\ K^{-1}$).[19,20] Therefore, an important strategy is to reduce thermal conductivity and maintain high power factor for higher

ZT. Particularly, reducing lattice thermal conductivity, which mainly contributes to the total high thermal conductivity, is an effective way for improving the *ZT* of TiS_2. Recently, Koumoto *et al.* used organic solvent molecules to intercalate TiS_2 single crystal and achieved ultralow in-plane lattice thermal conductivity of 0.12 W m^{-1} K^{-1}, resulting in a *ZT* value of ~0.2 at room temperature.[15] But intercalation of these molecules also led to significant decrease of the Seebeck coefficient and thus the power factor, as shown in Fig. 1a.[15,17,21] In addition, it is almost impossible to grow large-size TiS_2 single crystal for scalable production (for example, current single crystal TiS_2 is usually around 4 mm × 4 mm). In comparison, polycrystalline TiS_2 powders are suitable for mass-production and scalable solution processing. However, the thermoelectric properties of polycrystalline TiS_2 powders were much poorer, only 0.09 (*ZT*) at room temperature.[17] It will be of great interest to tune the polycrystalline TiS_2 powders so that their thermoelectric properties are comparable to the single crystal TiS_2.

Inclusion of nanostructures is very promising to improve the thermoelectric properties of polycrystalline TiS_2 films, which can greatly reduce the thermal conductivity via phonon scattering while slightly affecting the electron transport[22,23]. Significant progress has been made in thermoelectric materials via nanostructure-induced phonon scattering, such as BiSbTe alloys and PbTe.[24-29] Recent attempts indicated that, organic/inorganic hybrid nanostructures could demonstrate significantly-improved thermoelectric properties by reduction of thermal conductivity, such as graphene/skutterudite composites and carbon nanotubes/Cu_2Se composites recently.[30,31] Carbon nanocrystal, C_{60}, with extremely high Seebeck coefficient (-2000 μV K^{-1}) and low thermal conductivity (0.16 W m^{-1} K^{-1}) at room temperature[32-34] could be an ideal nanofiller to reduce the thermal conductivity of TiS_2 2D crystals while maintaining their high Seebeck coefficient and thus high power factor. However, to the best of our knowledge, no attempt has been reported to design and prepare such a novel C_{60}/TiS_2 hybrid nanostructure, and there is a lack of fundamental understanding on assembly, characterization, and thermoelectric properties of such novel hybrid nanostructures.

In this paper, we present liquid assembly of 0D C_{60} nanoparticles onto 2D TiS_2 nanosheets

to synthesize novel organic/inorganic heterostructures and study the thermoelectric properties of as-produced hybrids. Tailoring C_{60} nanoparticles increased the power factor of TiS_2 by >1.5-fold and also significantly decreased the thermal conductivity through the phonon scattering (Fig. 1a). As a result, the thermoelectric property of as-assembled C_{60}/TiS_2 hybrid films could rival that of the state-of-the-art TiS_2 single crystals.[15,21] As-produced novel hybrids can also be dispersed in the solvents and used as ink for printing large-area and flexible thermoelectric devices. A power density of 1.68 W m^{-2} for the printed device was achieved under a temperature gradient of 20 K (ΔT=20), which was much higher than that of reported thermoelectric devices based on organic materials or organic/inorganic composites (Fig. 1b).[6,13,18,35-37] Integration of solution-printability, air stability, and flexibility makes as-assembled C_{60}/TiS_2 hybrids a new class of flexible high-performance thermoelectric materials for flexible electronics.

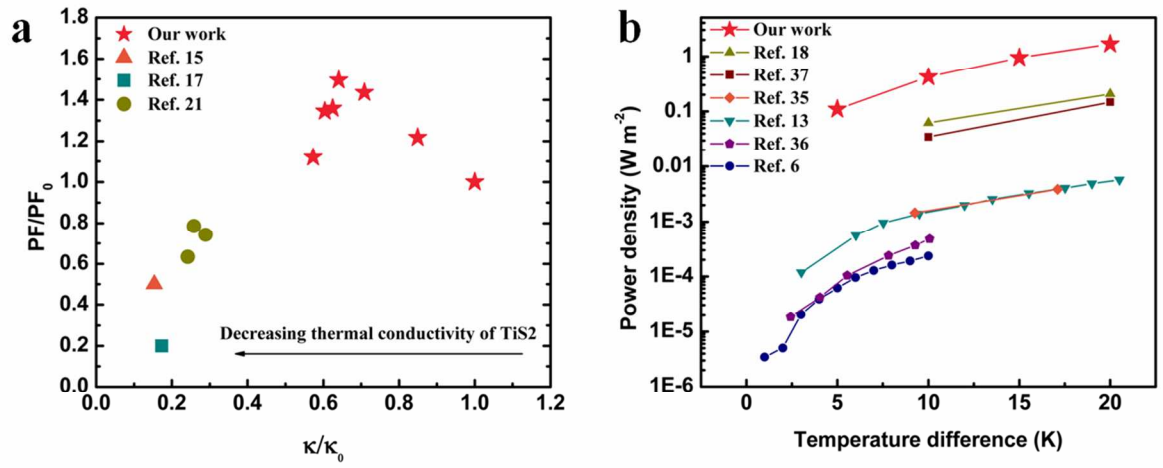

Fig. 1 (a) The variation of power factor with decreasing the thermal conductivity of TiS_2. PF_0 and κ_0 are the power factor and thermal conductivity of TiS_2, respectively. Typically, the decreases of thermal conductivity accompanies with the reduction in power factor[15,17,21]. In contrast, our work could demonstrate the simultaneous decrease in thermal conductivity and enhancement in power factor. (b) Comparisons of power density between the thermoelectric device of our work and reported thermoelectric devices based on organic materials or organic/inorganic composites.[6,13,18,35-37] The temperature differences are within 20 K which is easy to realize in a natural setting.

Results and discussion

Fabrication of C_{60}/TiS_2 hybrid films

Because of the significant solubility difference of C_{60} and TiS_2, directly mixing them in a common solvent is not possible for the assembly of C_{60}/TiS_2 hybrids. Hence, a facile liquid process via solvent transfer and surface deposition is developed to solve this problem, as illustrated in Fig. 2. In a typical procedure, TiS_2 nanosheets were dispersed into isopropyl alcohol (IPA), while a small amount of C_{60}/toluene solution was gradually injected into TiS_2/IPA solution under the assistance of bath sonication. Toluene and IPA are miscible, while the solubility of C_{60} in IPA is very low. Therefore, C_{60} nanoparticles gradually precipitated in IPA and preferably deposited on the hydrophobic surface of TiS_2 nanosheets because of the Van der Waals interaction.

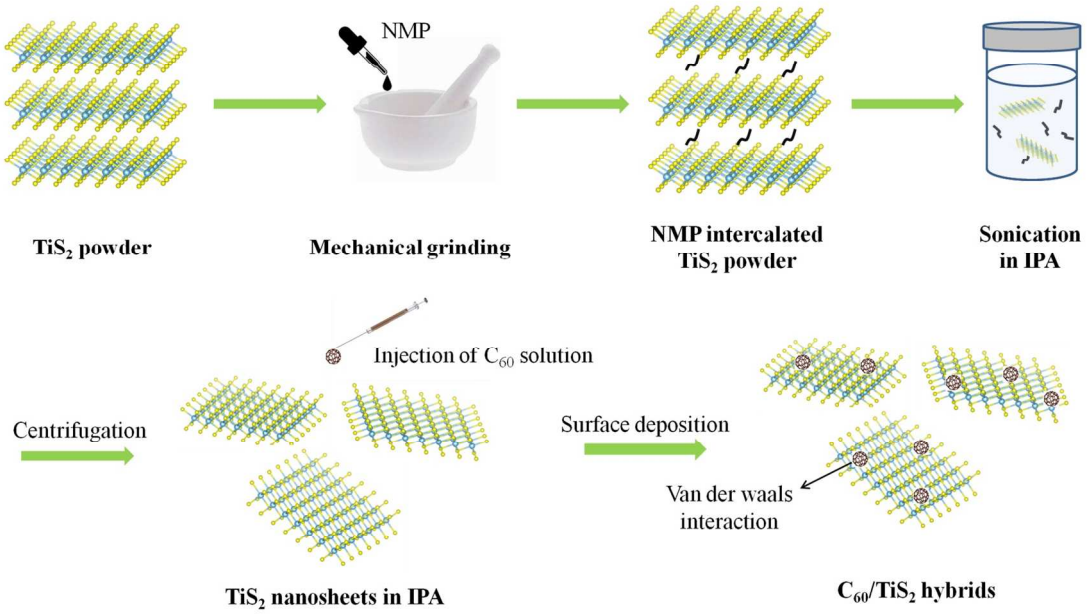

Fig. 2 Scheme of fabricating C_{60}/TiS_2 nanosheets hybrids by liquid process.

The composition and morphology of pristine TiS_2 powders were confirmed by X-ray diffraction (XRD) and scanning electron microscopy (SEM) results, as shown in Fig. S1 and Fig. S2. Exfoliated TiS_2 nanosheets were also characterized by atomic force microscope (AFM) (Fig.

3a and Fig. S3), and the cross-section analysis was carried out. The statistical distribution of exfoliated TiS_2 nanosheet thickness is shown in Fig. 3b, and most of them are less then 2 nm-thick, indicating single-layer or two-layer nanosheets. The transmission electron microscope (TEM) characterization indicated that as-exfoliated TiS_2 nanosheets showed a smooth and clean surface (Fig. 3c). In contrast, numerous small C_{60} nanoparticles were clearly observed on the surface of TiS_2 nanosheets for C_{60}-assembled TiS_2 hybrids as shown in Fig. 3d. The size of most C_{60} aggregates on TiS_2 nanosheets was around 5 nm. The C_{60}/TiS_2 suspension was very stable for more than one month, and can be used as ink to print large-area films. As-produced freestanding and flexible C_{60}/TiS_2 hybrid film is shown in Fig. 3e. The cross-section of such hybrid film was also characterized by SEM, clearly indicating the layered structures (Fig. 3f). As-produced C_{60}/TiS_2 hybrid film was also characterized by Raman spectroscopy. As shown in Fig. 3g, one peak at 334 cm^{-1} was observed in the spectra of both TiS_2 film and hybrid film. This low-frequency band was assigned to A_{1g} mode, corresponding to the vibration of sulfur atoms perpendicular to the sulfur layer. The features of the spectra are similar to those of 1T-TiS_2 (CdI_2 type structure).[38] Several characteristic peaks were observed in the Raman spectrum of C_{60}. In the Raman spectrum of hybrid film, both characteristic peaks of C_{60} and TiS_2 were observed, further confirming intercalation of C_{60} in the TiS_2 layers. The XRD characterization results of re-stacked TiS_2 film and C_{60}/TiS_2 nanosheets hybrid films are shown in Figure 3i. All the characteristic peaks observed in the XRD patterns are consistent with those in the reference PDF# 15-853.[39,40] The (001) peak of re-stacked TiS_2 film slightly shifted to a lower degree compared to pristine TiS_2 powders, indicating the increase of layer spacing. For the hybrid films, the (001) peak further shifted to a lower degree with the increasing C_{60} fractions. Obviously, the enlarged interlayer spacing was induced by the intercalation of C_{60} nanoparticles. The XRD peaks of C_{60} were not found for the hybrid samples, which was mainly due to the very low C_{60} amount. Similar phenomena were also reported in previous literatures.[41,42]

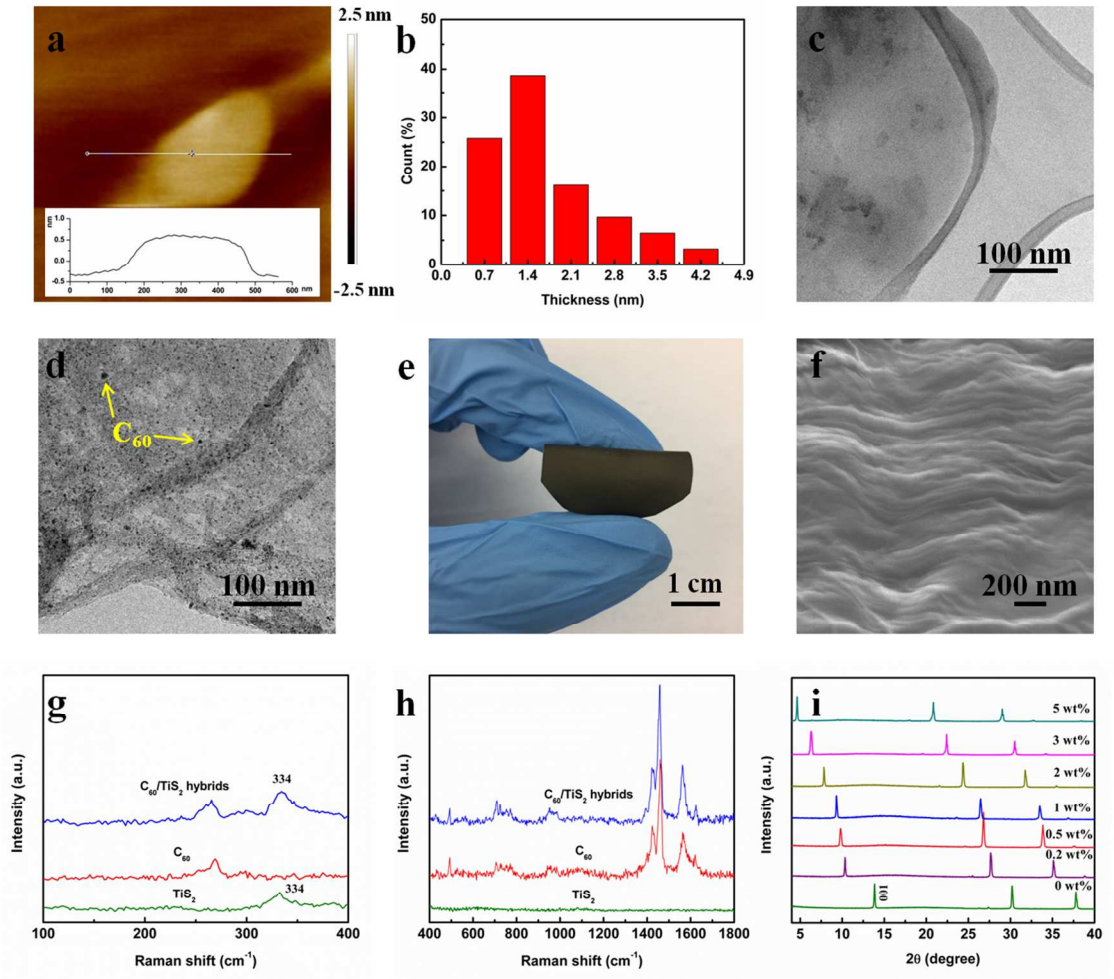

Fig. 3 Characterizations of synthesized C_{60}/TiS_2 nanosheets hybrid films. (a) Typical AFM image of exfoliated TiS_2 nanosheet. (b) The thickness distribution of exfoliated TiS_2 nanosheets. (c) TEM image of TiS_2 nanosheets. (d) TEM image of 1 wt% C_{60}/TiS_2 nanosheets hybrids. (e) Digital image of fabricated flexible C_{60}/TiS_2 nanosheets (1 wt% C_{60} content) hybrid film in a large area of 3 cm × 3 cm. (f) Cross-sectional SEM image of fabricated 1 wt% C_{60}/TiS_2 nanosheets hybrid film. (g, h) Raman spectra of TiS_2 film, C_{60} powders, and 1 wt% C_{60}/TiS_2 nanosheets hybrid film. (i) XRD patterns of TiS_2 film and C_{60}/TiS_2 nanosheets hybrid films with different C_{60} content.

Thermoelectric performance

The electrical conductivity and Seebeck coefficient of prepared films were characterized as a function of C_{60} fractions in the in-plane direction at room temperature and the results are shown in Fig. 4a and Fig. 4b. The re-stacked TiS_2 films showed electrical conductivity of ~480 S cm^{-1}

and Seebeck coefficient of ~-75 μV K^{-1}. After assembling C_{60} nanoparticles on the surface of TiS_2 nanosheets, the electrical conductivity persistently decreased while the Seebeck coefficient increased with an increasing C_{60} amount. When the C_{60} amount was 1 wt%, the Seebeck coefficient of hybrid films reached -101 μV K^{-1}. At further increase of the C_{60} amount, the enhancement in Seebeck coefficient was very slight. This may be casued by the aggregation of $C_{60.}$ Because of the limited surface on the TiS_2 nanosheets, continuous adding C_{60} above 1wt% could force them to aggregate to form larger clusters, as indicated by the XRD results in Fig. 3i. The carrier concentration of fabricated films was measured and is shown in Fig. S8, which decreased with the increasing C_{60} content. The influence of the varied carrier concentration on the Seebeck coefficient was evaluated by the Pisarenko plot[43], as shown in Fig. S9. Our experimental results of the Seebeck coefficient for the hybrid films were larger than those calculated values, indicating that reduction of carrier concentration only partially contributed to the enhancement of Seebeck coefficient. Some other factors, such as C_{60} components and interfacial scattering, could also significantly contribute to the enhancement of Seebeck coefficient.[44] A maximum power factor of as high as ~400 μW m^{-1} K^{-2} was observed in C_{60}/TiS_2 hybrid films at 1 wt% C_{60}, which is much higher than that of the re-stacked TiS_2 films, and previously reported n-type TMD polycrystalline films (see Table S2).[17,18,45,46] These results have confirmed that it is feasible to maintain or even enhance the high thermoelectric power factor of TiS_2 by C_{60} intercalation. As-fabricated C_{60}/TiS_2 hybrid film also demonstrates a good flexibility, as shown in Fig. 4d. The increase of electrical resistance for 1 wt% C_{60}/TiS_2 hybrid film was within 5% even at a bending radius of 3.5 mm. The stability of prepared C_{60}/TiS_2 hybrid film was also investigated. As illustrated in Fig. S10, the hybrid film demonstrated negligible changes in both the electrical conductivity and Seebeck coefficient during the testing.

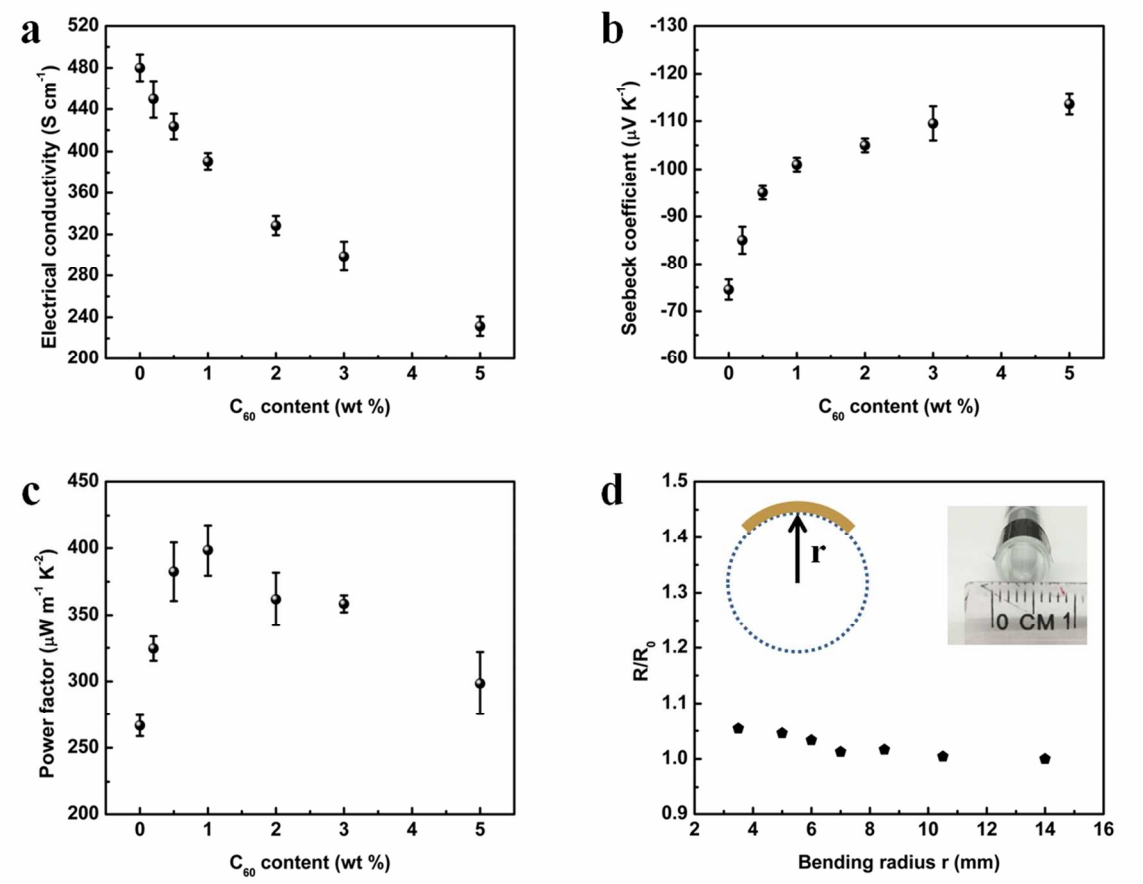

Fig. 4 In-plane thermoelectric properties of fabricated TiS_2 film and C_{60}/TiS_2 nanosheets hybrid films as a function of C_{60} content, and the air stability of hybrid film. (a) Electrical conductivity. (b) Seebeck coefficient. (c) power factor. (d) The resistance R of the 1 wt% C_{60}/TiS_2 hybrid film as a function of bending radius r, where R_0 is the resistance before bending. The resistance were measured by attaching hybrid film onto glass tube with different diameter.

More impressively, inclusion of C_{60} nanoparticles onto the surface of TiS_2 nanosheets can also significantly decrease the thermal conductivity (especially the lattice thermal conductivity) of TiS_2 because of the phonon scattering. The in-plane thermal conductivity was characterized by a laser flash method, and is shown in Fig. 5a. When the C_{60} content was increased to 1 wt% in the hybrid film, the thermal conductivity dramatically decreased from 0.96 W m^{-1} K^{-1} to 0.61 W m^{-1} K^{-1}, almost 36% reduction. However, further increasing C_{60} content only led to little reduction in thermal conductivity. The lattice thermal conductivity (κ_L) can be calculated by subtracting the carrier part κ_e from the total κ, where κ_e is calculated by the Wiedemann-Franz

law ($\kappa_e = L_0\sigma T$). L_0 is the Lorentz number and can be given as follows,

$$L_0 = (\frac{k_B}{e})^2 (\frac{(r+7/2)F_{(r+5/2)}(\eta)}{(r+3/2)F_{(r+1/2)}(\eta)} - \left[\frac{(r+5/2)F_{(r+3/2)}(\eta)}{(r+3/2)F_{(r+1/2)}(\eta)}\right]^2), \quad (1)$$

where k_B is the Boltzmann constant, e is the electron charge, r is the scattering factor, and η is the reduced Fermi energy. The dominant scattering mechanism of TiS_2 is acoustic phonon scattering, so r = -1/2.[15] The reduced Fermi energy η should be derived from the measured Seebeck coefficients,

$$S = \pm\frac{k_B}{e}(\frac{(r+5/2)F_{(r+3/2)}(\eta)}{(r+3/2)F_{(r+1/2)}(\eta)} - \eta), \quad (2)$$

where $F_n(\eta)$ is the n^{th}-order Fermi integral,

$$F_n(\eta) = \int_0^\infty \frac{\chi^n}{1+e^{\chi-\eta}} d\chi. \quad (3)$$

The calculated lattice thermal conductivities are shown in Fig. 5b. Similar to the trend of total thermal conductivity, the lattice thermal conductivity of hybrid film rapidly decreased to 0.39 W m^{-1} K^{-1} at 1 wt% C_{60}, and then decreased very slightly with increasing C_{60} content. The thermal conductivity of TiS_2 single crystal was as high as ~6.8 W m^{-1} K^{-1}, while the thermal conductivity of sintered TiS_2 polycrystals was reported to be ~3.4 W m^{-1} K^{-1}.[19,47,48] In comparison, the thermal conductivity of as-fabricated C_{60}/TiS_2 hybrid films was very low. Previous work showed that ultralow in-plane thermal conductivity of ~0.7 W m^{-1} K^{-1} and lattice thermal conductivity of ~0.12 W m^{-1} K^{-1} can be achieved by using organic molecules to intercalate TiS_2 single crystal.[15] In this work, the significant reduction of thermal conductivity can be attributed to the phonon scattering induced by the grain boundary between TiS_2 nanosheets and C_{60} nanoparticles. As illustrated in Fig. 5c, the grain boundary of TiS_2 nanosheets can effectively scatter the long-wavelength phonons. The smaller-size C_{60} nanoparticles preferably scatter the mid-wavelength and short-wavelength phonons. As mentioned above, there was a limited surface area to assemble C_{60} nanoparticles on each TiS_2 nanosheet. Therefore, high fraction of C_{60} nanoparticles tended to aggregate and thus cannot effectively increase the number of phonon

scatter centers, resulting in slow decrease of thermal conductivity. Based on the experimental measurements, the *ZT* value (~300 K) was as high as 0.2 for 1 wt% C_{60}/TiS_2 nanosheets hybrid films, which is comparable to the state-of-the-art TiS_2 single crystals.[15,21]

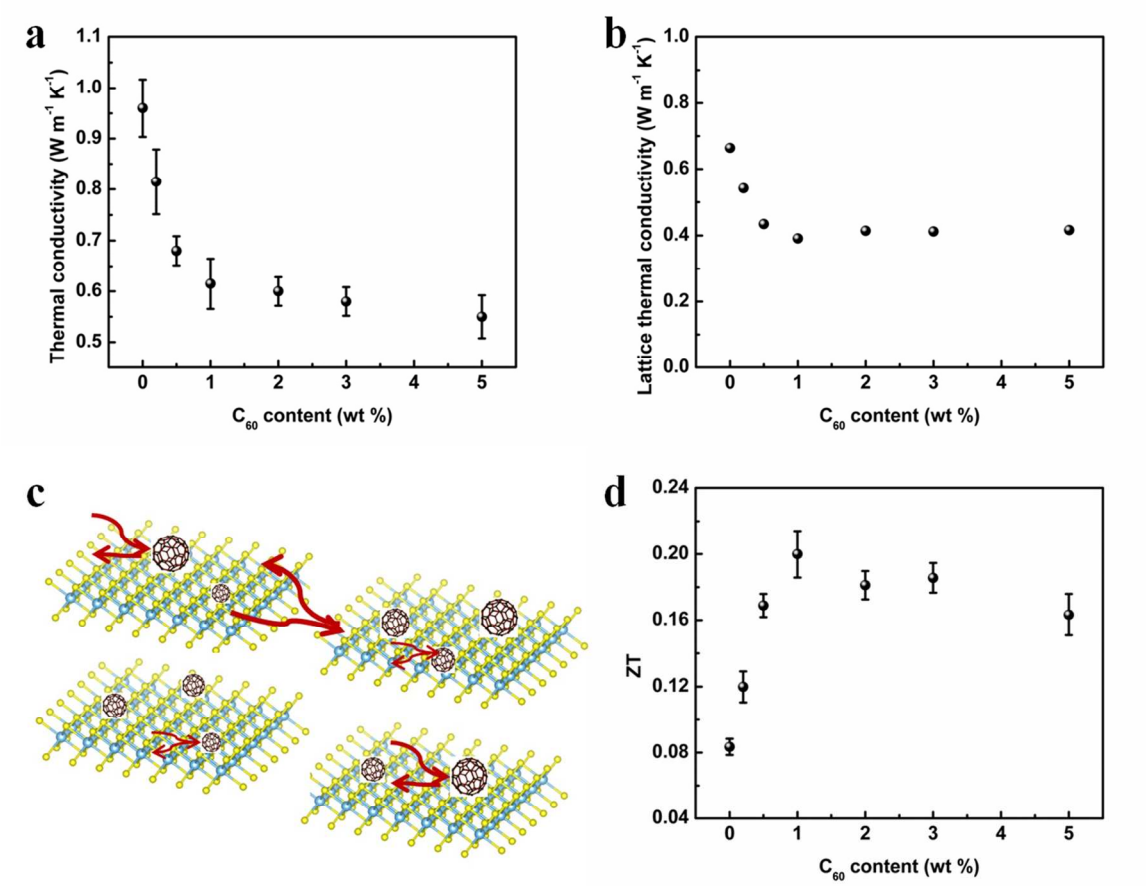

Fig. 5 In-plane thermoelectric properties of fabricated TiS_2 film and C_{60}/TiS_2 nanosheets hybrid films as a function of C_{60} content. (a) Thermal conductivity. (b) Lattice thermal conductivity. (c) Schematic illustration of phonon scattering in C_{60}/TiS_2 nanosheets hybrid films. (d) *ZT* versus C_{60} fraction.

The temperature-dependent thermoelectric properties of TiS_2 film and 1 wt% C_{60}/TiS_2 hybrid film are shown in Fig. 6. The electrical conductivities of both TiS_2 film and hybrid film decreased with the increasing temperature, displaying metallic conductive behavior. This changing trend is consistent with recent publications on organic molecules intercalated TiS_2 materials.[15,21] In contrast to the electrical conductivity, the Seebeck coefficients of both TiS_2 film and hybrid film increased with the increasing temperature. As a result, the power factor of TiS_2

film stayed stable with the increasing temperature while the power factor of C_{60}/TiS_2 hybrid film decreased slightly with the increasing temperature, from ~400 μW m^{-1} K^{-2} at ~300 K to 375 μW m^{-1} K^{-2} at ~400 K. Overall, C_{60}/TiS_2 hybrid films demonstrated much larger power factor than that of TiS_2 film in the whole temperature range of measurement. The temperature-dependent thermal conductivities including lattice thermal conductivities of the two films are shown in Fig. 6d. It was clearly observed that assembling C_{60} nanoparticles onto TiS_2 nanosheets greatly decreased both the total thermal conductivity and lattice thermal conductivity of TiS_2. Moreover, the total thermal conductivity of the hybrid film slightly decreased with the increasing temperature. As a result, the *ZT* value of 1 wt% C_{60}/TiS_2 hybrid film increased to 0.3 at 400 K. The thermoelectric properties of the state-of-the-art n-type organic materials and organic/inorganic hybrid materials were summarized in Fig. 6f, including organic intercalated TMDs[15,17,21], metal coordination polymers[13,14], insulating polymer/metal composites[49], and PEI doped carbon nanotubes[50]. The *ZT* value of as-prepared C_{60}/TiS_2 polycrystalline flexible films is compatible to that of the single crystal TiS_2 materials, and among the highest level of the flexible n-type thermoelectric materials.

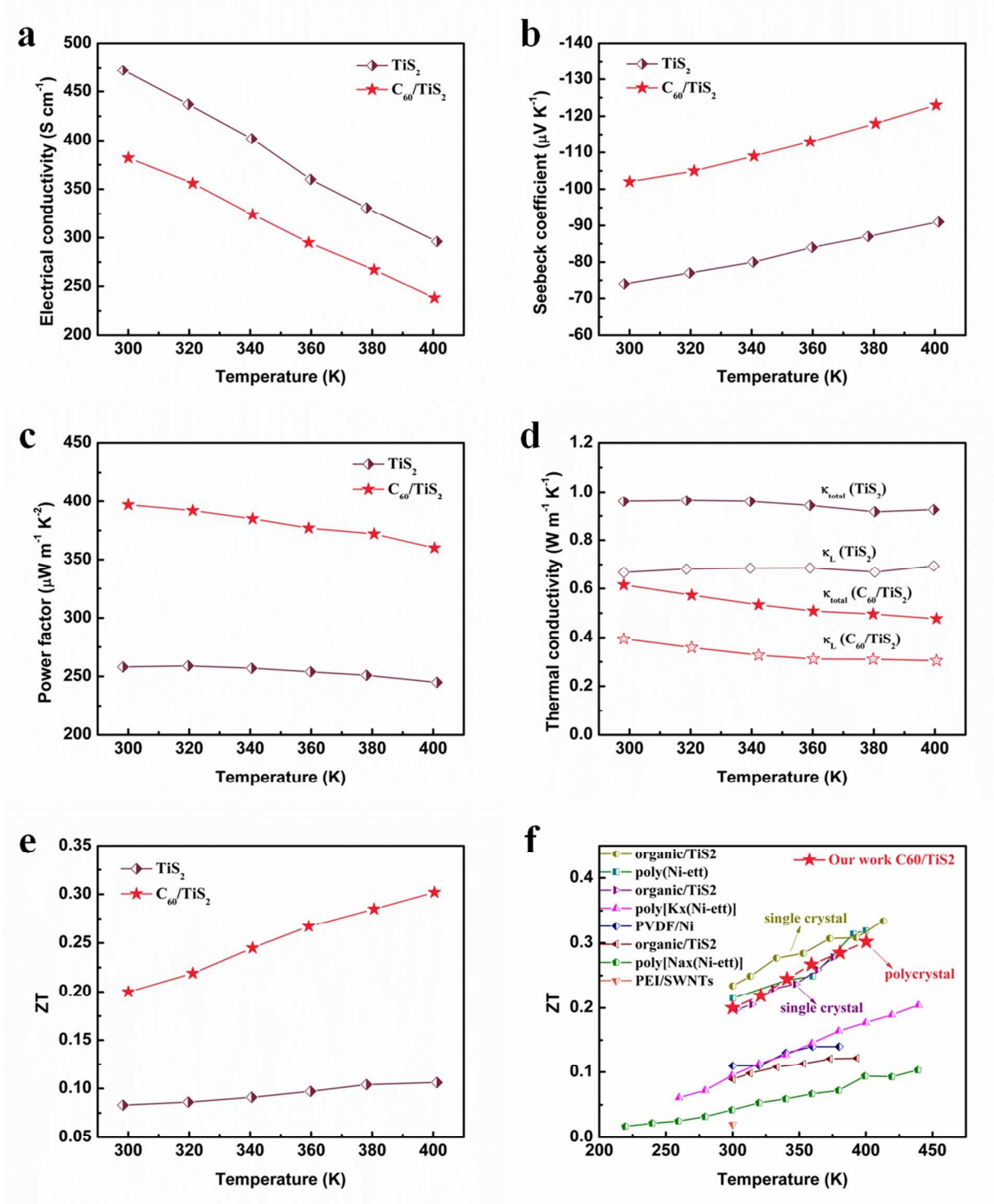

Fig. 6 High-temperature in-plane thermoelectric properties of fabricated TiS_2 film and 1 wt% C_{60}/TiS_2 nanosheets hybrid film. (a) Electrical conductivity. (b) Seebeck coefficient. (c) power factor. (d) Total thermal conductivity and lattice thermal conductivity. (e) *ZT*. (f) Comparisons of *ZT* values for state-of-the-art flexible

and printable organic thermoelectrics and organic/inorganic hybrid thermoelectrics.[13-15,17,21,49,50]

Device performance

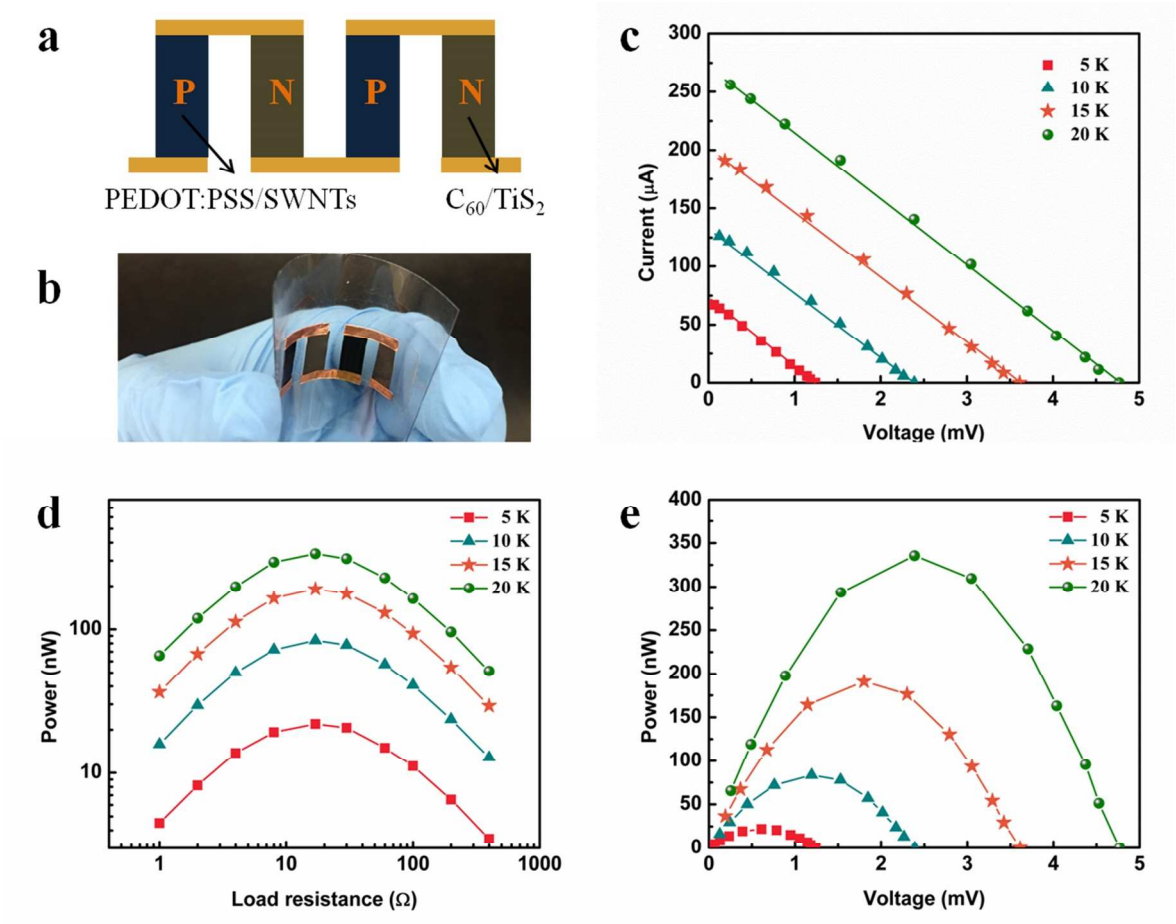

Fig. 7 Photograph and performance of fabricated device. (a) Schematic illustration of the thermoelectric device consisting of 50 wt% SWNTs/PEDOT:PSS films (p-type legs) and 1 wt% C_{60}/TiS_2 hybrid films (n-type legs). (b) Corresponding photograph of fabricated device with good flexibility. (c) The current-voltage curve of the device at different temperature difference. (d) The generated power of the device as a function of load resistance. (e) The power-voltage curve of the device at different temperature difference.

Owing to the good processibility, as-prepared C_{60}/TiS_2 hybrids are suitable for scalable, cost-effective, high-rate and continuous solution process, and thus it is convenient to fabricate large-area flexible thermoelectric devices by printing techniques such as roll-to-roll printing reported by our group[51]. A flexible thermoelectric module composed of parallel connected 4 legs

was fabricated using 1 wt% C_{60}/TiS_2 hybrid films as n-type legs while 50 wt% single-walled carbon nanotubes (SWNTs)/PEDOT:PSS hybrid films were used as p-type legs, as shown in Fig. 7b. Each component leg was 10 mm in length, 5 mm in width, and 10 μm in thickness. The electrical resistance of as-fabricated device was measured to be 16.6 Ω. In principle, the output voltage of thermoelectric device can be given by $U = E - IR_{in}$, where E is the open-circuit voltage of the device, R_{in} is the resistance of the device, and I is the output current. Hence, the output voltage is inversely proportional to the output current at a certain temperature gradient. As shown in Fig. 7c, the output current-voltage curves were plotted against different temperature gradients by connecting the device with external load resistance in series. An inverse relationship was observed between current and voltage, and the output voltages increase with the increasing temperature difference, reaching ~4.8 mV at a temperature difference of 20 K. The output power (P) can be expressed as, $P = EI - I^2R_{in} = E^2R/(R + R_{in})^2$, where R is the load resistance. Therefore, the maximum output power can be obtained when the external load resistance matches the inner resistance of the device. As shown in Fig. 7d, output powers were plotted against the external load resistance. Under all the temperature gradient, the output powers reached maximum when the load resistance was about 17 Ω, well matching the inner resistance of the device. In addition, the output powers were parabolic as a function of the output current (Fig. 7e). The maximum output power was about 335 nW at a temperature difference of 20 K. By dividing the cross-sectional area and the number of legs, the normalized maximum power density was 1.68 W m^{-2}, which is superior to the reported thermoelectric devices based on organic materials or organic/inorganic composites under a similar temperature difference.[6,13,18,35-37]

Conclusions

In summary, we demonstrate a facile approach to synthesize novel organic/inorganic heterostructures of C_{60}-intercalated TiS_2. Assembling 0D C_{60} nanoparticles onto 2D TiS_2 nanosheets not only significantly increased the Seebeck coefficient and the power factor, but also reduced the thermal conductivity of TiS_2. The resultant ZT was ~0.3 at 400 K, and compatible to the single crystal TiS_2 materials, which are very expensive, difficult to synthesize, and incapable

of solution printing. This method can be extended to other TMDs for creating high-performance n-type thermoelectric materials. More importantly, as-assembled organic/inorganic hybrid can serve as ink for scalable printing flexible and air-stable n-type legs in the thermoelectric devices. These results will significantly facilitate the utilization of thermoelectric devices in the field of flexible electronics.

Experimental

Materials. The pristine TiS_2 powders were synthesized via solid-state reaction by heating stoichiometric mixtures of Ti and S as reported in previous paper[39]. N-Methyl-2-pyrrolidone (NMP), Isopropy alcohol (IPA) and toluene were purchased from Sigma-Aldrich. C_{60} powders were purchased from Cheap Tubes Inc.. PEDOT:PSS (PH 1000) was purchased from Clevios. All the materials were used as received.

Liquid assembly of C_{60}/TiS_2 nanosheets hybrids. For the fabrication process of C_{60}/TiS_2 nanosheets hybrids, 0.2 g synthesized TiS_2 powders and 0.2 mL NMP were thoroughly mixed and manually ground with a pestle for 30 min. The powders were then transferred into a glass beaker with 40 mL IPA and ultra-sonicated in a bath sonicator for 3 h. Afterwards, the solution was centrifuged for 30 min at 4000 rpm for twice to completely remove the bulk powders. The supernatant containing TiS_2 nanosheets was collected for further use. Various amount (0.2 wt%, 0.5 wt%, 1 wt%, 2 wt%, 3 wt%, 5 wt%) of 1 mg mL^{-1} C_{60} toluene solution was then slowly added into 30 mL 1 mg mL^{-1} TiS_2 nanosheets IPA solution, in order to deposit C_{60} onto the surface of TiS_2 nanosheets. The mixture was further ultra-sonicated for 30 min to facilitate the surface deposition process.

Film preparation. As-prepared solution containing C_{60}/TiS_2 nanosheets hybrids can be printed onto substrates or vacuum filtrated with filter membranes to obtain free-standing films. All the films were dried in a vacuum oven at 45 ^oC for 1 h to achieve C_{60}/TiS_2 hybrid films. Then, the obtained C_{60}/TiS_2 hybrid films were annealed at 150 ^oC for 1 h, in order to remove the residual organic solvent molecules.

Device fabrication. P-type ink was prepared by homogeneously dispersing 50 wt% SWNTs into

PEDOT:PSS with a probe sonicator. Suspension containing 1 wt% C_{60}/TiS_2 hybrids was used as n type ink. The flexible plastic substrate was treated by oxygen plasma for one hour before fabrication device. Both p-type ink and n-type ink could be processed onto plastic substrate with desired patterns. At last, p-type legs and n-type legs were connected with conductive metals.

Characterizations. The morphologies of prepared TiS_2 nanosheets and C_{60}/TiS_2 hybrids were characterized by transmission electron microscopy (TEM, JEOL JEM-2010). As-fabricated films were also characterized by atomic force microscope (AFM, Bruker), X-ray diffraction (XRD, Bruker D8) with a Cu-K_a source (wavelength of 1.54056Å), and Raman spectrometer (Jobin-Yvon HORIBA LabRAM HR800 instrument coupled to an Olympus BX41 microscopy, $\lambda_{exc.}$ = 514.5 nm). The film thickness was measured by a Dektak profilometer. The electrical conductivity and Seebeck coefficient were measured along the in-plane direction at room temperature with home-built apparatus (see Electronic Supplementary Information). The carrier concentration and mobility were measured according to the Hall effect in a Physics Property Measurements System (PPMS, Quantum Design). The high-temperature electrical conductivity and Seebeck coefficient of films were measured with ZEM-3 (ULVAC-RLKO). The mechanical flexibility was assessed by attaching the films on glass tubes with different diameter and testing their resistances as function of tube radius. The in-plane thermal diffusivity (λ) of film was tested by LFA 447 (Netzsch) with a special sample holder (Fig. S11). The heat capacity (C_p) was measured using the differential scanning calorimetry in the temperature range of 300 K - 400 K. Then the thermal conductivity (κ) of film was obtained from the relationship $\kappa = \rho\lambda C_p$ (ρ was the density). The out-of-plane thermal conductivity was also measured by LFA 447 for comparison. For the characterization of device performance, temperature difference was produced by heating one side of the device with a resistance heater, and a voltage meter (Keithley 2182A) was used to recorded the generated thermoelectric voltage (Fig. S14).

Data availability. Data that support the findings of this study are available from the corresponding author upon reasonable request.

References

1. Snyder, G. J. & Toberer, E. S. Complex thermoelectric materials. *Nat. Mater.* **7**, 105-114 (2008).

2. Du, Y., Shen, S. Z., Cai, K. & Casey, P. S. Research progress on polymer-inorganic thermoelectric nanocomposite materials. *Prog. Polym. Sci.* **37**, 820-841 (2012).
3. Zhou, Y. & Zhao, L. D. Promising thermoelectric bulk materials with 2D structures. *Adv. Mater.* **29**, 1702676 (2017).
4. Tan, G., Zhao, L. D. & Kanatzidis, M. G. Rationally designing high-performance bulk thermoelectric materials. *Chem. Rev.* **116**, 12123-12149 (2016).
5. Zhang, X. & Zhao, L. D. Thermoelectric materials: Energy conversion between heat and electricity. *J. Materiomics* **1**, 92-105 (2015).
6. Bubnova, O. et al. Optimization of the thermoelectric figure of merit in the conducting polymer poly(3,4-ethylenedioxythiophene). *Nat. Mater.* **10**, 429-433 (2011).
7. Kim, G. H., Shao, L., Zhang, K. & Pipe, K. P. Engineered doping of organic semiconductors for enhanced thermoelectric efficiency. *Nat. Mater.* **12**, 719-723 (2013).
8. Bubnova, O. et al. Semi-metallic polymers. *Nat. Mater.* **13**, 190-194 (2014).
9. Avery, A. D. et al. Tailored semiconducting carbon nanotube networks with enhanced thermoelectric properties. *Nat. Energy* **1**, 16033 (2016).
10. Russ, B., Glaudell, A., Urban, J. J., Chabinyc, M. L. & Segalman, R. A. Organic thermoelectric materials for energy harvesting and temperature control. *Nat. Rev. Mater.* **1**, 16050 (2016).
11. Russ, B. et al. Power Factor Enhancement in Solution-Processed Organic n-Type Thermoelectrics Through Molecular Design. *Adv. Mater.* **26**, 3473-3477 (2014).
12. Schlitz, R. A. et al. Solubility-Limited Extrinsic n-Type Doping of a High Electron Mobility Polymer for Thermoelectric Applications. *Adv. Mater.* **26**, 2825-2830 (2014).
13. Sun, Y. et al. Organic Thermoelectric Materials and Devices Based on p- and n-Type Poly(metal 1,1,2,2-ethenetetrathiolate)s. *Adv. Mater.* **24**, 932-937 (2012).
14. Sun, Y. et al. Flexible n-Type High-Performance Thermoelectric Thin Films of Poly(nickel-ethylenetetrathiolate) Prepared by an Electrochemical Method. *Adv. Mater.* **28**, 3351-3358 (2016).
15. Wan, C. L. et al. Flexible n-type thermoelectric materials by organic intercalation of layered transition metal dichalcogenide TiS2. *Nat. Mater.* **14**, 622-627 (2015).
16. Wan, C. L. et al. Dielectric Mismatch Mediates Carrier Mobility in Organic-Intercalated Layered TiS2. *Nano Lett.* **15**, 6302-6308 (2015).
17. Wan, C. L. et al. Flexible thermoelectric foil for wearable energy harvesting. *Nano Energy* **30**, 840-845 (2016).
18. Tian, R. M. et al. A solution-processed TiS2/organic hybrid superlattice film towards flexible thermoelectric devices. *J. Mater. Chem. A* **5**, 564-570 (2017).
19. Imai, H., Shimakawa, Y. & Kubo, Y. Large thermoelectric power factor in TiS2 crystal with nearly stoichiometric composition. *Phys. Rev. B* **64,** 241104 (2001).
20. Daou, R. et al. Intrinsic effects of substitution and intercalation on thermal transport in two-dimensional TiS2 single crystals. *J. Appl. Phys.* **117,** 165101 (2015).
21. Wan, C. et al. Ultrahigh thermoelectric power factor in flexible hybrid inorganic-organic superlattice. *Nat. Commun.* **8**, 1024 (2017).
22. Hicks, L. D. & Dresselhaus, M. S. THERMOELECTRIC FIGURE OF MERIT OF A

ONE-DIMENSIONAL CONDUCTOR. *Phys. Rev. B* **47**, 16631-16634 (1993).

23. Hicks, L. D. & Dresselhaus, M. S. EFFECT OF QUANTUM-WELL STRUCTURES ON THE THERMOELECTRIC FIGURE OF MERIT. *Phys. Rev. B* **47**, 12727-12731 (1993).
24. Zhao, L. D. et al. All-scale hierarchical thermoelectrics: MgTe in PbTe facilitates valence band convergence and suppresses bipolar thermal transport for high performance. *Energy Environ. Sci.* **6**, 3346-3355 (2013).
25. Biswas, K. et al. High-performance bulk thermoelectrics with all-scale hierarchical architectures. *Nature* **489**, 414-418 (2012).
26. Vineis, C. J., Shakouri, A., Majumdar, A. & Kanatzidis, M. G. Nanostructured Thermoelectrics: Big Efficiency Gains from Small Features. *Adv. Mater.* **22**, 3970-3980 (2010).
27. Lan, Y. C. et al. Structure Study of Bulk Nanograined Thermoelectric Bismuth Antimony Telluride. *Nano Lett.* **9**, 1419-1422 (2009).
28. Poudel, B. et al. High-thermoelectric performance of nanostructured bismuth antimony telluride bulk alloys. *Science* **320**, 634-638 (2008).
29. Ma, Y. et al. Enhanced thermoelectric figure-of-merit in p-type nanostructured bismuth antimony tellurium alloys made from elemental chunks. *Nano Lett.* **8**, 2580-2584 (2008).
30. Zong, P.-a. et al. Skutterudite with graphene-modified grain-boundary complexion enhances zT enabling high-efficiency thermoelectric device. *Energy Environ. Sci.* **10**, 183-191 (2017).
31. Nunna, R. et al. Ultrahigh thermoelectric performance in Cu2Se-based hybrid materials with highly dispersed molecular CNTs. *Energy Environ. Sci.* **10**, 1928-1935 (2017).
32. Zhang, K., Zhang, Y. & Wang, S. R. Enhancing thermoelectric properties of organic composites through hierarchical nanostructures. *Sci. Rep.* **3,** 3448 (2013).
33. Sumino, M. et al. Thermoelectric properties of n-type C-60 thin films and their application in organic thermovoltaic devices. *Appl. Phys. Lett.* **99,** 093308 (2011).
34. Paloheimo, J., Isotalo, H., Kastner, J. & Kuzmany, H. CONDUCTION MECHANISMS IN UNDOPED THIN-FILMS OF C60 AND C60/70. *Synth. Met.* **56**, 3185-3190 (1993).
35. Suemori, K., Hoshino, S. & Kamata, T. Flexible and lightweight thermoelectric generators composed of carbon nanotube-polystyrene composites printed on film substrate. *Appl. Phys. Lett.* **103,** 153902 (2013).
36. Zhang, K., Qiu, J. J. & Wang, S. R. Thermoelectric properties of PEDOT nanowire/PEDOT hybrids. *Nanoscale* **8**, 8033-8041 (2016).
37. Wang, L., Yao, Q., Shi, W., Qu, S. & Chen, L. Engineering carrier scattering at the interfaces in polyaniline based nanocomposites for high thermoelectric performances. *Mater. Chem. Front.* **1,** 741-748 (2017).
38. Carmalt, C. J., O'Neill, S. A., Parkin, I. P. & Peters, E. S. Titanium sulfide thin films from the aerosol-assisted chemical vapour deposition of [Ti(SBut)4]. *J. Mater. Chem.* **14**, 830-834 (2004).
39. Geng, L. et al. Titanium Sulfides as Intercalation-Type Cathode Materials for Rechargeable Aluminum Batteries. *ACS Appl. Mater. Interfaces* **9**, 21251-21257 (2017).
40. Sun, W. et al. “Water-in-Salt” electrolyte enabled LiMn2O4/TiS2 Lithium-ion batteries. *Electrochem. Commun.* **82**, 71-74 (2017).
41. Yu, J., Ma, T., Liu, G. & Cheng, B. Ehanced photocatalytic activity of bimodal mesoporous titania powders by C60 modification. *Dalton Trans.* **40,** 6635-6644 (2011).
42. Chai, B., Liao, X., Song, F. & Zhou, H. Fullerene modified C3N4 composites with enhanced photocatalytic activity under visible light irradiation. *Dalton Trans.* **43,** 982-989 (2014).

43. Zhang, J. et al. Thermoelectric properties of TiS2-xPbSnSe3 nanocomposites. *J. Alloys Compd.* **696**, 1342-1348 (2017).
44. Faleev, S. V. & Leonard, F. Theory of enhancement of thermoelectric properties of materials with nanoinclusions. *Phys. Rev. B* **77**, 214304 (2008).
45. Oh, J. Y. et al. Chemically exfoliated transition metal dichalcogenide nanosheet-based wearable thermoelectric generators. *Energy Environ. Sci.* **9**, 1696-1705 (2016).
46. Jo, K., Choi, J. & Kim, H. Benzyl viologen-assisted simultaneous exfoliation and n-doping of MoS2 nanosheets via a solution process. *J. Mater. Chem. C* **5**, 5395-5401 (2017).
47. Ye, Y. et al. Enhanced thermoelectric performance of xMoS2-TiS2 nanocomposites. *J. Alloys Compd.* **666**, 346-351 (2016).
48. Guilmeau, E., Barbier, T., Maignan & Chateigner, D. Thermoelectric anisotropy and texture of intercalated TiS_2. *Appl. Phys. Lett.* **111**, 133903 (2017).
49. Chen, Y. et al. Bendable n-Type Metallic Nanocomposites with Large Thermoelectric Power Factor. *Adv. Mater.* **29**, 1604752 (2017).
50. Zhou, W. et al. High-performance and compact-designed flexible thermoelectric modules enabled by a reticulate carbon nanotube architecture. *Nat. Commun.* **8**, 14886 (2017).
51. Zhang, Z., Qiu, J. & Wang, S. Roll-to-roll printing of flexible thin-film organic thermoelectric devices. *Manuf. Lett.* **8**, 6-10 (2016).

Acknowledgements

The authors appreciate the support from startup funds of Texas A&M University and TEES, and also partial support from the National Science Foundation grant (CMMI 1634858).

Competing interests

The authors no competing financial interests.

Additional information

Electronic Supplementary Information is available for this paper.

Broader context

More than half of industrial energy is lost as waste heat, and thus it is critical to recycle waste heat for efficient energy utilization. Thermoelectrics involving the conversion between heat and electricity can recycle such waster heat in a safe and environmentally friendly manner. Thermoelectrics can also produce clean energy by harvesting thermal energy from sustainable resources, and facilitate water reuse for global sustainability. They also have great potential for high-precision thermal sensors and non-invasive or minimally-invasive therapy. Contrary from conventional rigid thermoelectrics, flexible thermoelectrics show a huge advantage of easy integration in versatile formats but are limited by their inferior thermoelectric properties. In this paper, we demonstrate n-type fullerene/TiS_2 organic/inorganic hybrid films which integrate mechanical flexibility, solution-printability and outstanding thermoelectric properties together. Our work opens a new door for utilizing flexible thermoelectric materials in the field of stretchable electronics, flexible power generator, tunable water-reuse systems, and adaptable sensors.

Graphical abstract

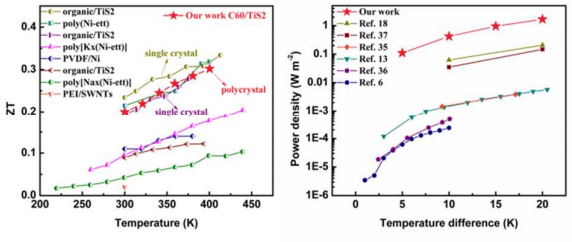

Flexible and solution-printable fullerene/TiS_2 organic/inorganic hybrids with excellent thermoelectric properties are demonstrated.